

## Supporting Information

# Zinc(II)-Heteroligand Compounds for Wet Processing OLEDs: A Study on Balancing Charge-Carrier Transport and Energy Transfer

*Emmanuel Santos Moraes,<sup>1,2†</sup> Luís Gustavo Teixeira Alves Duarte,<sup>2†</sup> Fabiano Severo Rodembusch,<sup>3</sup> José Carlos Germino,<sup>1\*</sup> Luiz Fernando Ribeiro Pereira<sup>1\*</sup> and Teresa Dib Zambon Atvars<sup>2\*</sup>.*

<sup>1</sup>Department of Physics and i3N-Institute for Nanostructures, Nanomodelling and Nanofabrication, University of Aveiro, 3810-193 Aveiro, Portugal

<sup>2</sup>Chemistry Institute, University of Campinas, Campinas 13083-970, Brazil.

<sup>3</sup>Grupo de Pesquisa em Fotoquímica Orgânica Aplicada, Instituto de Química (UFRGS), Av. Bento Gonçalves, 9500, CEP 91501-970 Porto Alegre, RS, Brazil

†Authors that contribute equally to this work.

\*Corresponding Author. E-mail: [germino@ua.pt](mailto:germino@ua.pt), [luiz@ua.pt](mailto:luiz@ua.pt) and [tatvars@unicamp.br](mailto:tatvars@unicamp.br)

## Summary

<b>Figure S1.</b> $^1\text{H}$ NMR in DMSO- $d_6$ of the complex <b>ZnL11</b> .....	1
<b>Figure S2.</b> $^1\text{H}$ NMR in DMSO- $d_6$ of the complex <b>ZnL22</b> .....	1
<b>Figure S3.</b> $^1\text{H}$ NMR in DMSO- $d_6$ of the complex <b>ZnL13</b> .....	2
<b>Figure S4.</b> $^1\text{H}$ NMR in DMSO- $d_6$ of the complex <b>ZnL23</b> .....	2
<b>Figure S5.</b> $^{13}\text{C}$ NMR in DMSO- $d_6$ of the complex <b>ZnL11</b> .....	3
<b>Figure S6.</b> $^{13}\text{C}$ NMR in DMSO- $d_6$ of the complex <b>ZnL22</b> .....	3
<b>Figure S7.</b> $^{13}\text{C}$ NMR in DMSO- $d_6$ of the complex <b>ZnL13</b> .....	4
<b>Figure S8.</b> $^{13}\text{C}$ NMR in DMSO- $d_6$ of the complex <b>ZnL23</b> .....	4
<b>Figure S9.</b> FTIR spectra of all Zinc(II) complexes.....	5
<b>Figure S10.</b> HRMS of the complex <b>ZnL11</b> .....	6
<b>Figure S11.</b> HRMS of the complex <b>ZnL22</b> .....	6
<b>Figure S12.</b> HRMS of the complex <b>ZnL13</b> .....	7
<b>Figure S13.</b> HRMS of the complex <b>ZnL23</b> .....	7
<b>Figure S14.</b> TGA thermograms of all complexes.....	8
<b>Figure S15.</b> Zn(II)-homo and heteroligands HOMO and LUMO frontier molecular orbitals... <b>Figure S16.</b> Spectral overlap between Zn(II) coordination compounds absorption/excitation and PFO photoluminescence spectra at solid-state and thin-film, respectively.....	9
<b>Table S1.</b> Summary of time-resolved photoluminescence data used for FRET's efficiencies calculations.....	10
<b>Figure S17.</b> Photoluminescence decay curves of (a) <b>ZnL13</b> and (b) <b>ZnL23</b> at different concentrations in PFO matrix.....	10
<b>Figure S18.</b> Thin film photoluminescence spectra of the Zn(II) coordination compounds excited into PFO matrix ( $\lambda_{\text{exc}}=375$ nm), where: (a) <b>ZnL22</b> ; (b) <b>ZnL23</b> ; and (c) <b>ZnL13</b> .....	11
<b>Figure S19.</b> Mott-Gurney's, Child's and Mark-Helfrich's space-charge electrical transport models adjusts applied to PFO:ZnL11 (1 % mol/mol) OLED current density versus voltage curve and their fit parameters.....	12
<b>Figure S20.</b> Mott-Gurney's, Child's and Mark-Helfrich's space-charge electrical transport models adjusts applied to PFO:ZnL11 (1 % mol/mol) OLED current density versus voltage curve and their fit parameters.....	13
<b>Figure S21.</b> Mott-Gurney's, Child's and Mark-Helfrich's space-charge electrical transport models adjusts applied to PFO:ZnL11 (1 % mol/mol) OLED current density versus voltage curve and their fit parameters.....	14
<b>Figure S22.</b> Mott-Gurney's, Child's and Mark-Helfrich's space-charge electrical transport models adjusts applied to PFO:ZnL11 (1 % mol/mol) OLED current density versus voltage curve and their fit parameters.....	15

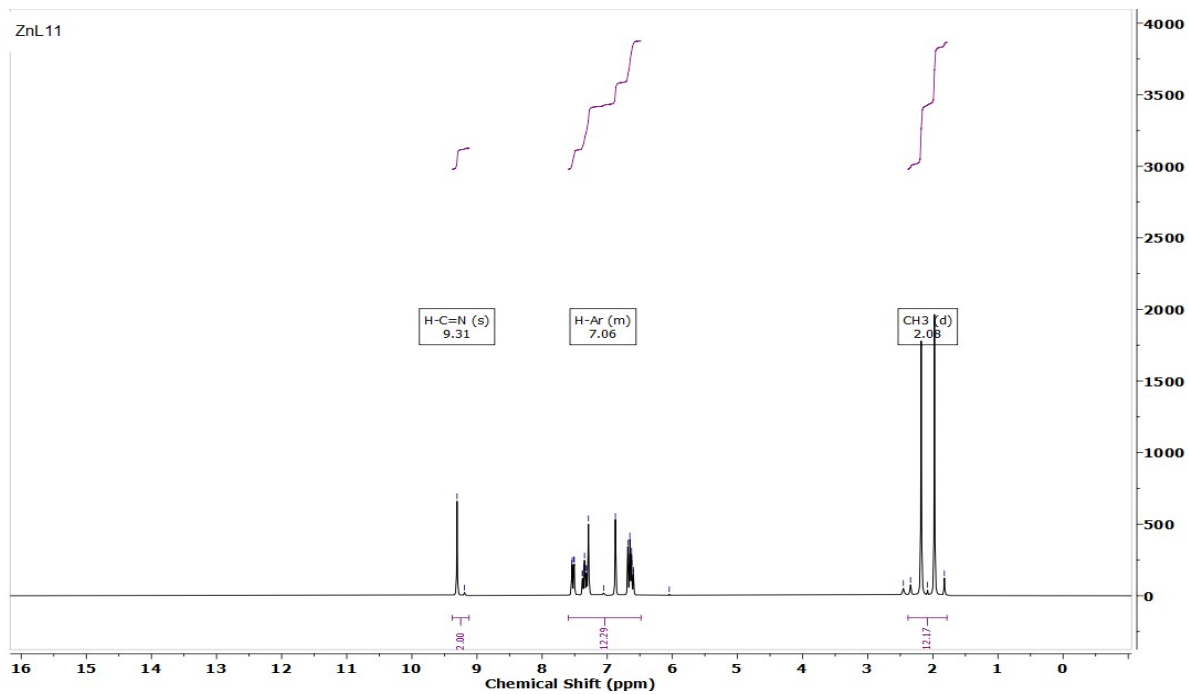


**Figure S1.**  $^1\text{H}$  NMR in  $\text{DMSO}-d_6$  of the complex ZnL11.

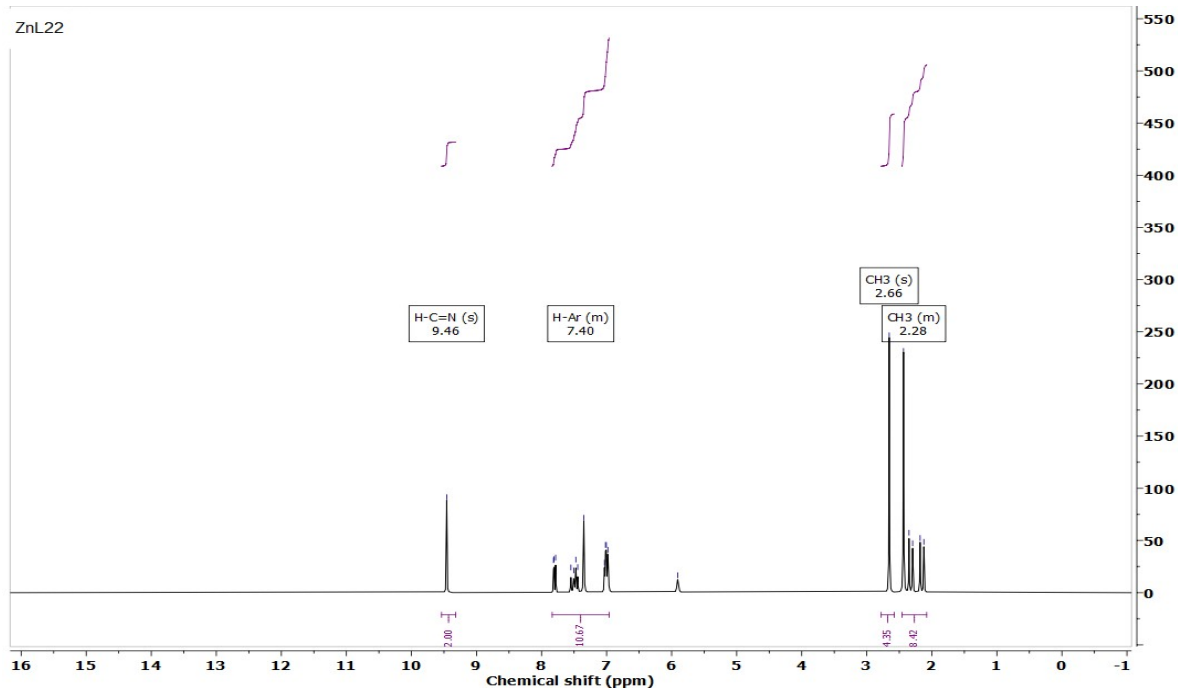


**Figure S2.**  $^1\text{H}$  NMR in  $\text{DMSO}-d_6$  of the complex ZnL22.

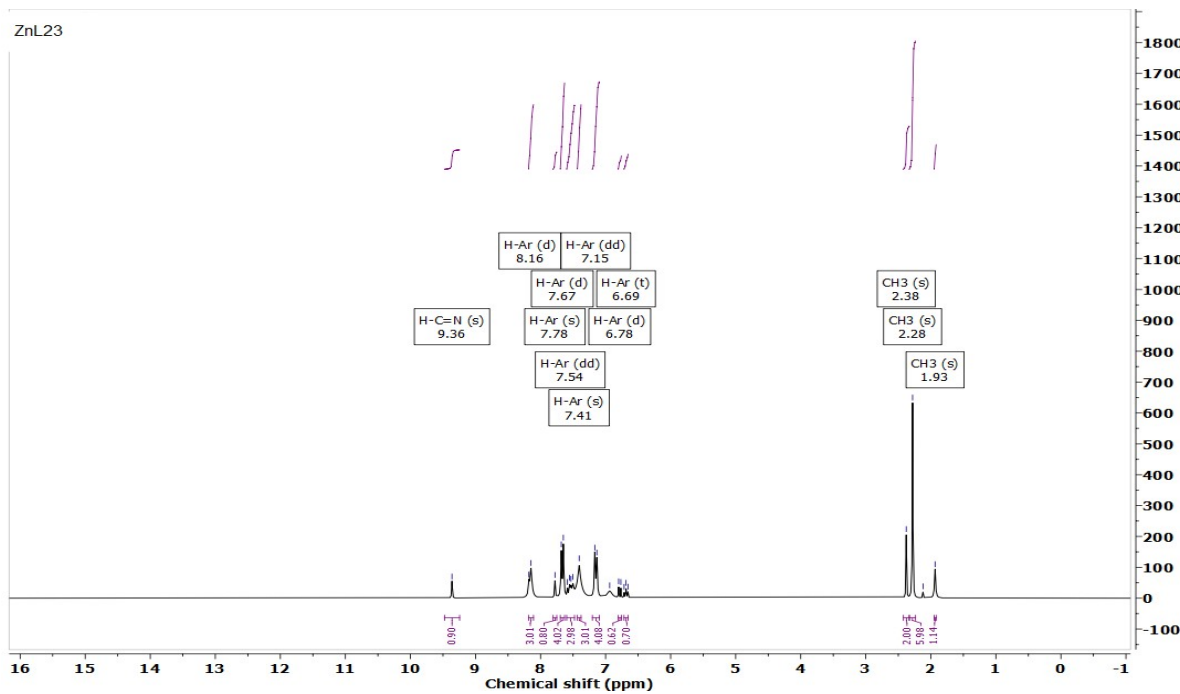


**Figure S3.**  $^1\text{H}$  NMR in  $\text{DMSO}-d_6$  of the complex **ZnL13**.

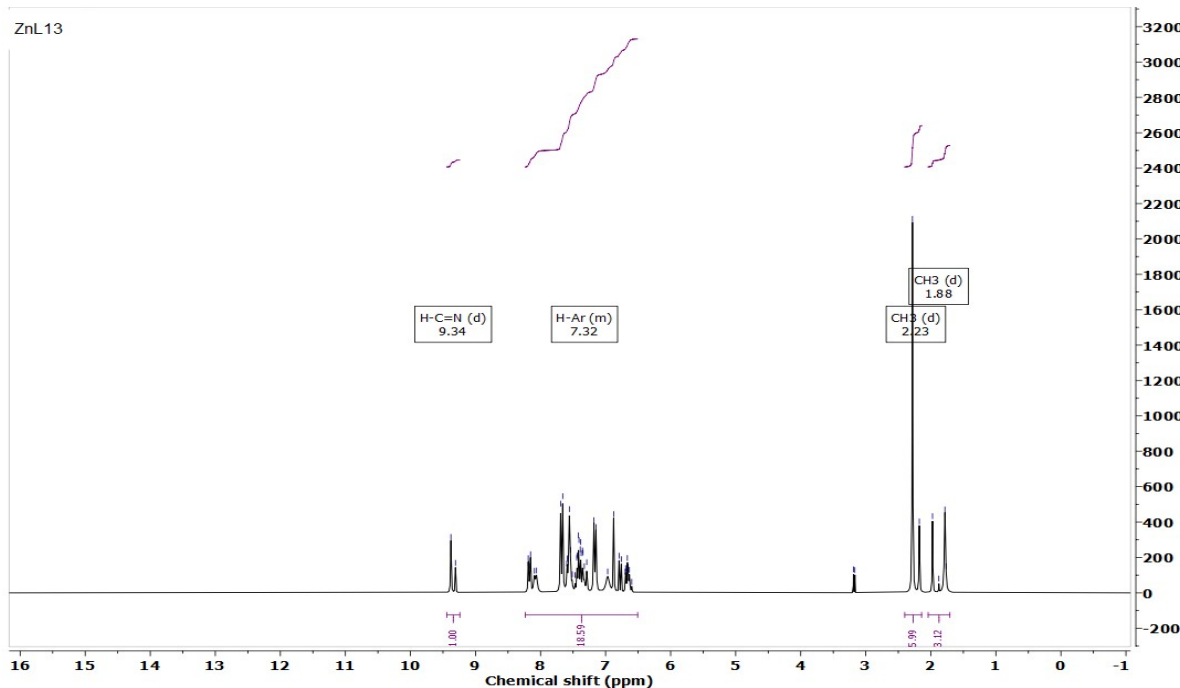


**Figure S4.**  $^1\text{H}$  NMR in  $\text{DMSO}-d_6$  of the complex **ZnL23**.

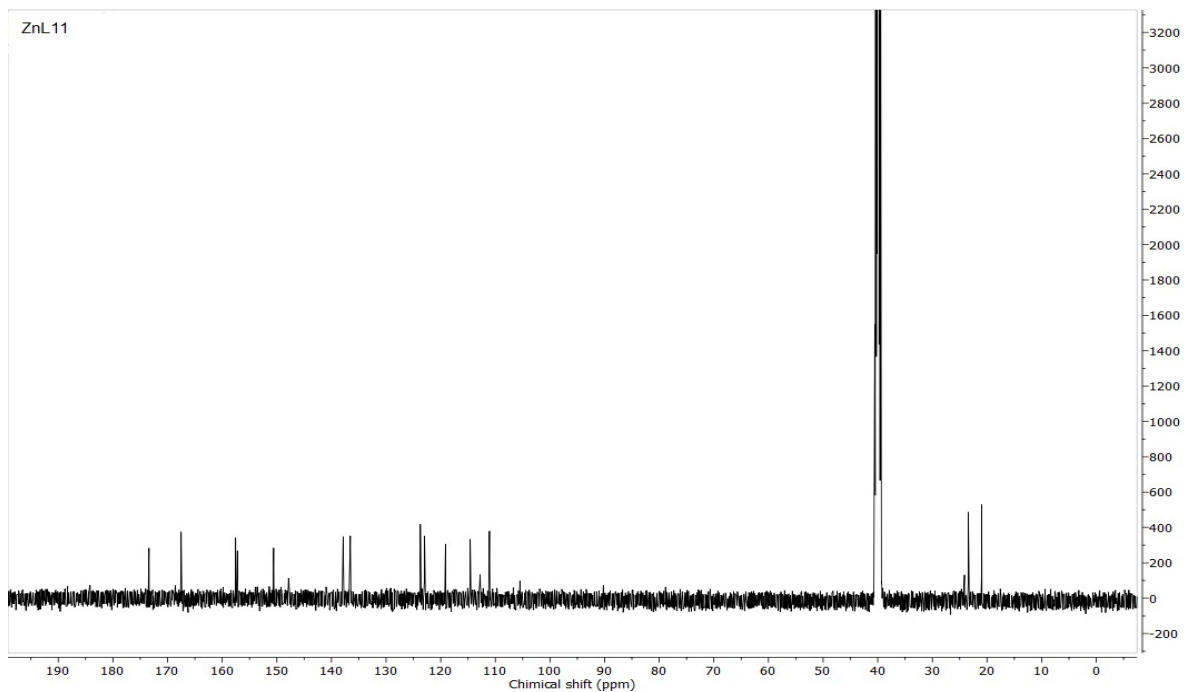


**Figure S5.** <sup>13</sup>C NMR in DMSO-*d*<sub>6</sub> of the complex **ZnL11**.

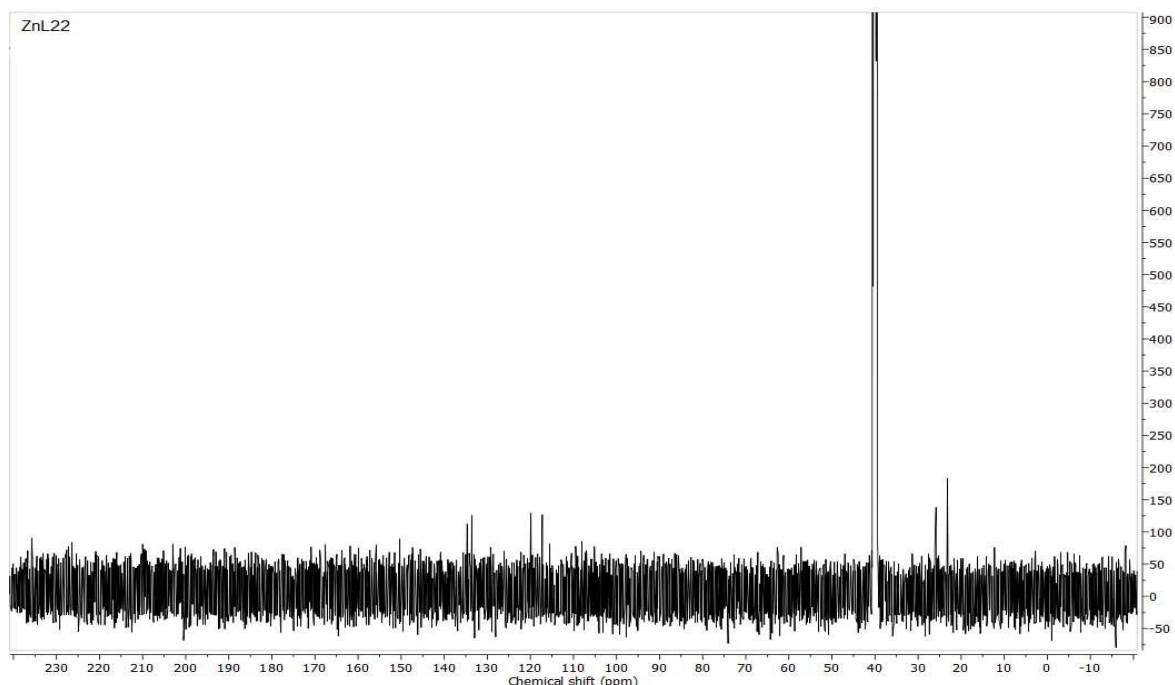


**Figure S6.** <sup>13</sup>C NMR in DMSO-*d*<sub>6</sub> of the complex **ZnL22**.

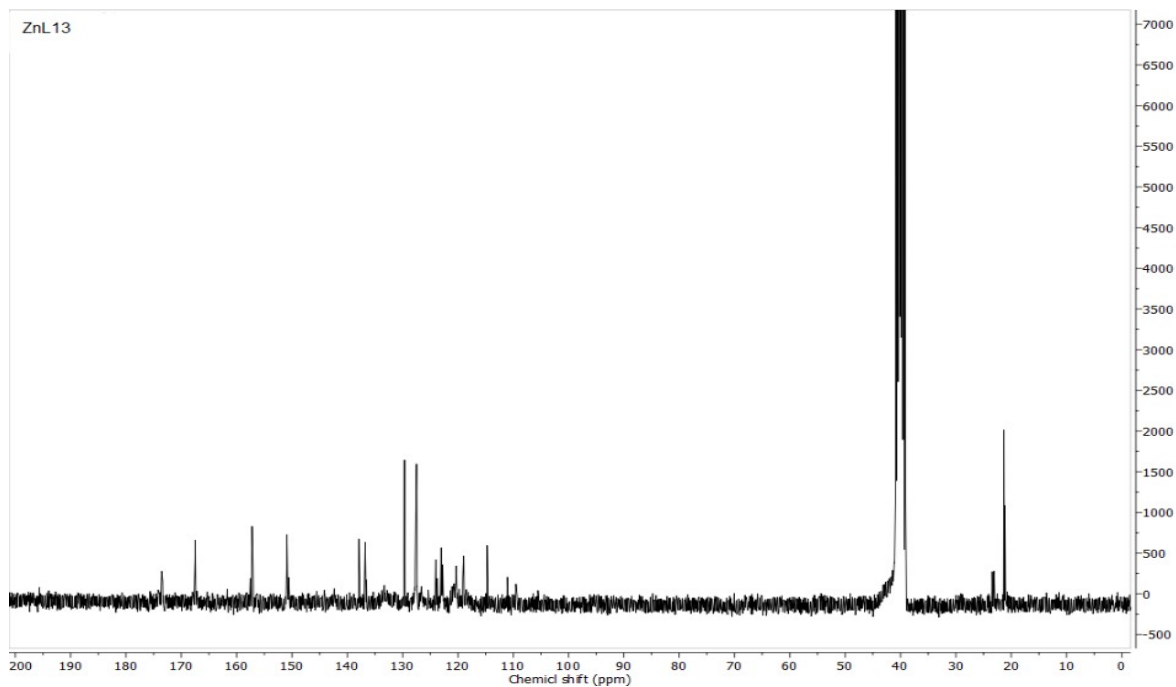


**Figure S7.** <sup>13</sup>C NMR in DMSO-*d*<sub>6</sub> of the complex **ZnL13**.

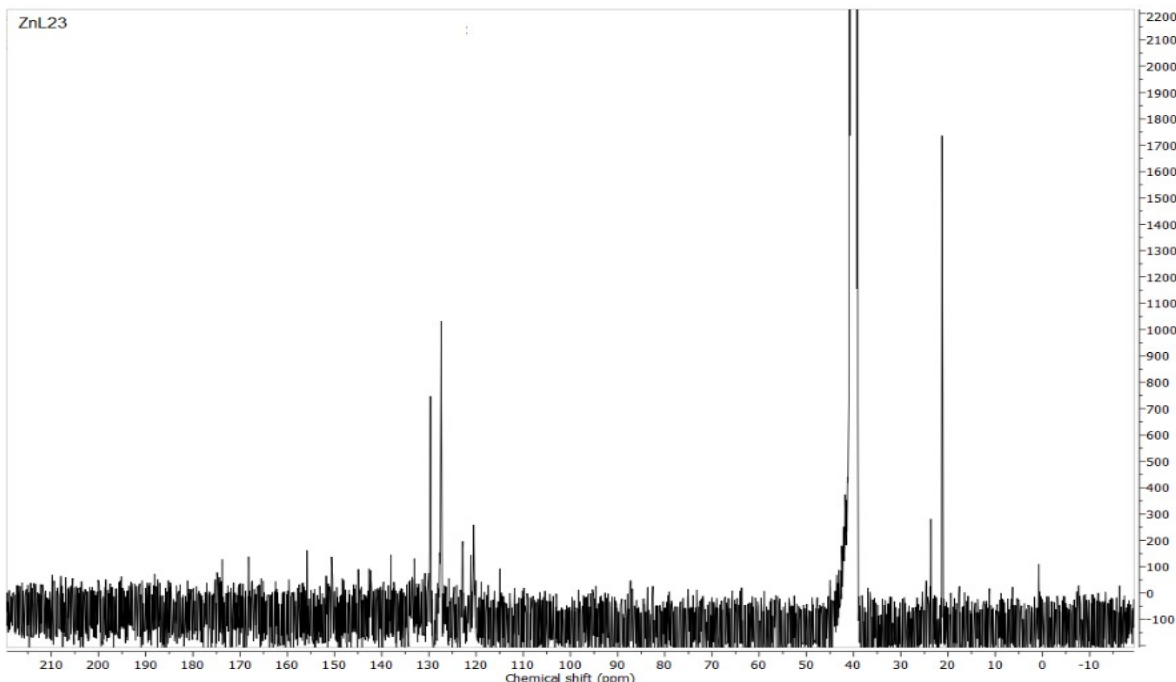


**Figure S8.** <sup>13</sup>C NMR in DMSO-*d*<sub>6</sub> of the complex **ZnL23**.

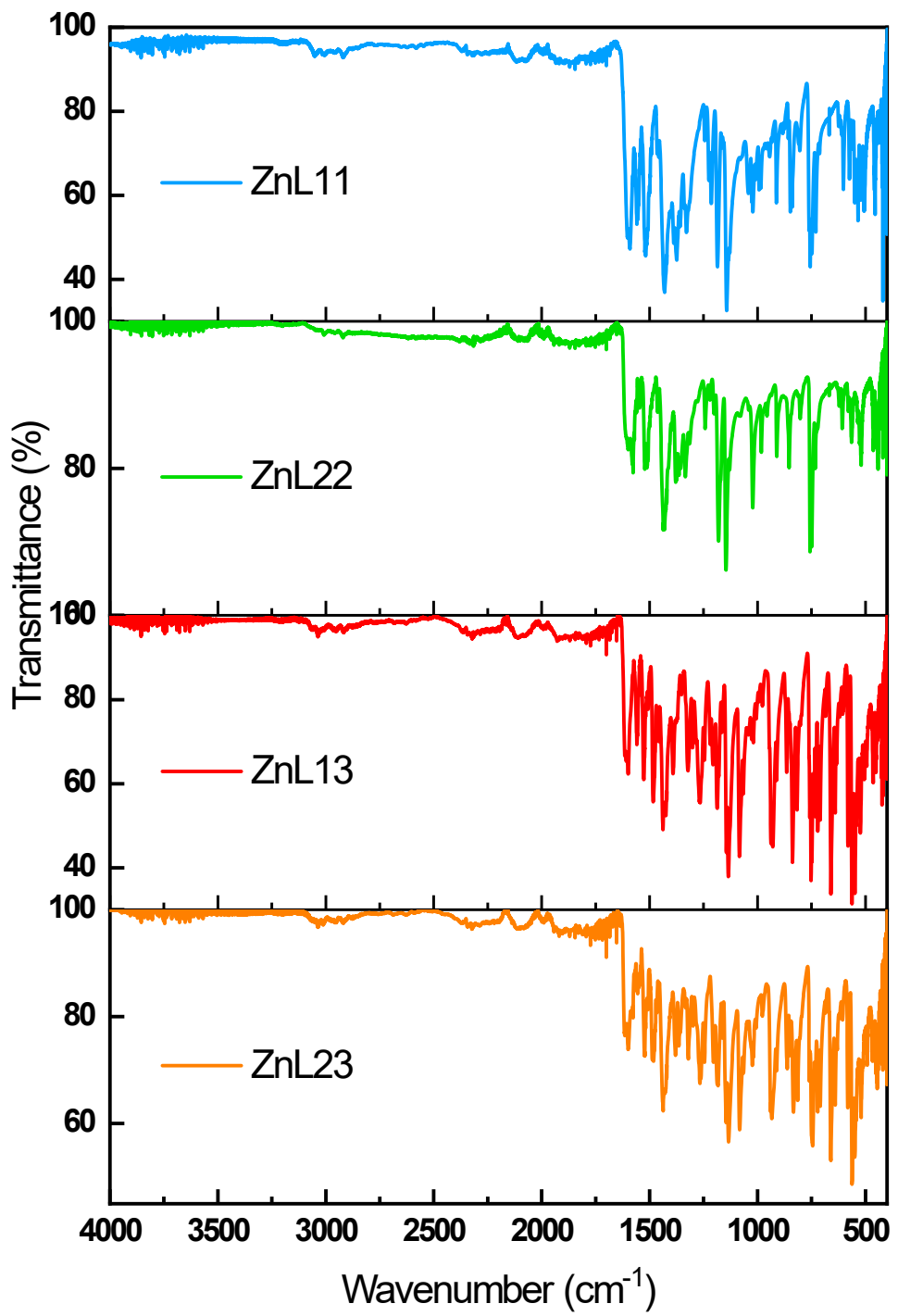


**Figure S9.** FTIR spectra of all Zinc(II) complexes.

Espectro completo de 100 a 1000 m/z em modo positivo

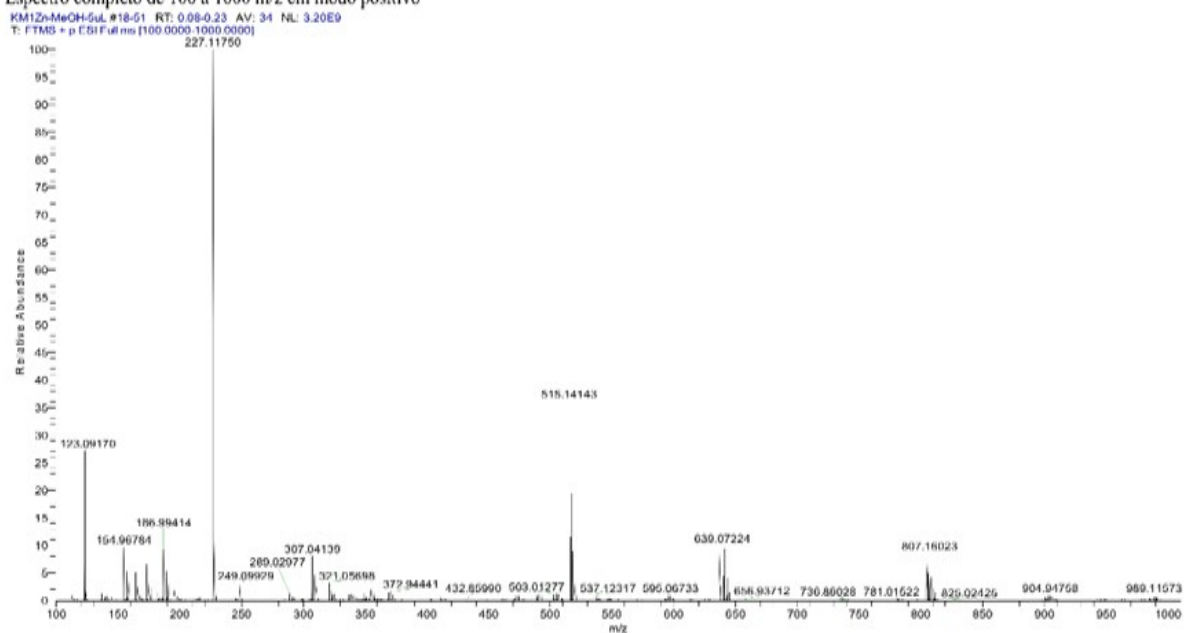


**Figure S10.** HRMS of the complex ZnL11.

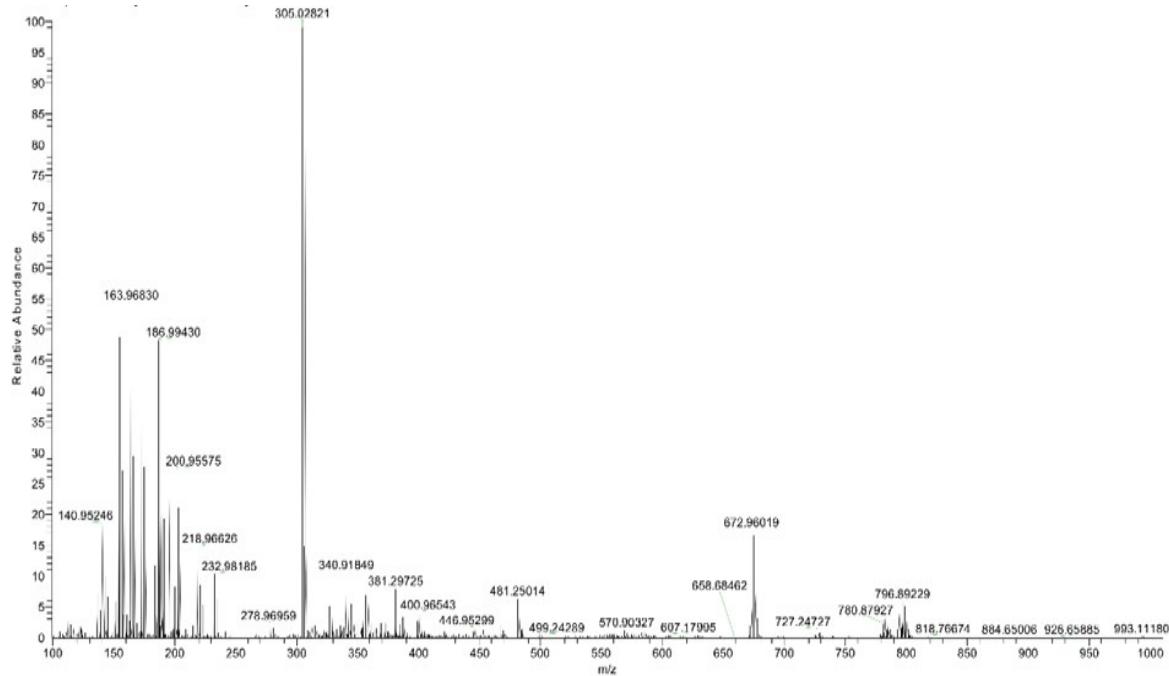


**Figure S11.** HRMS of the complex ZnL22.

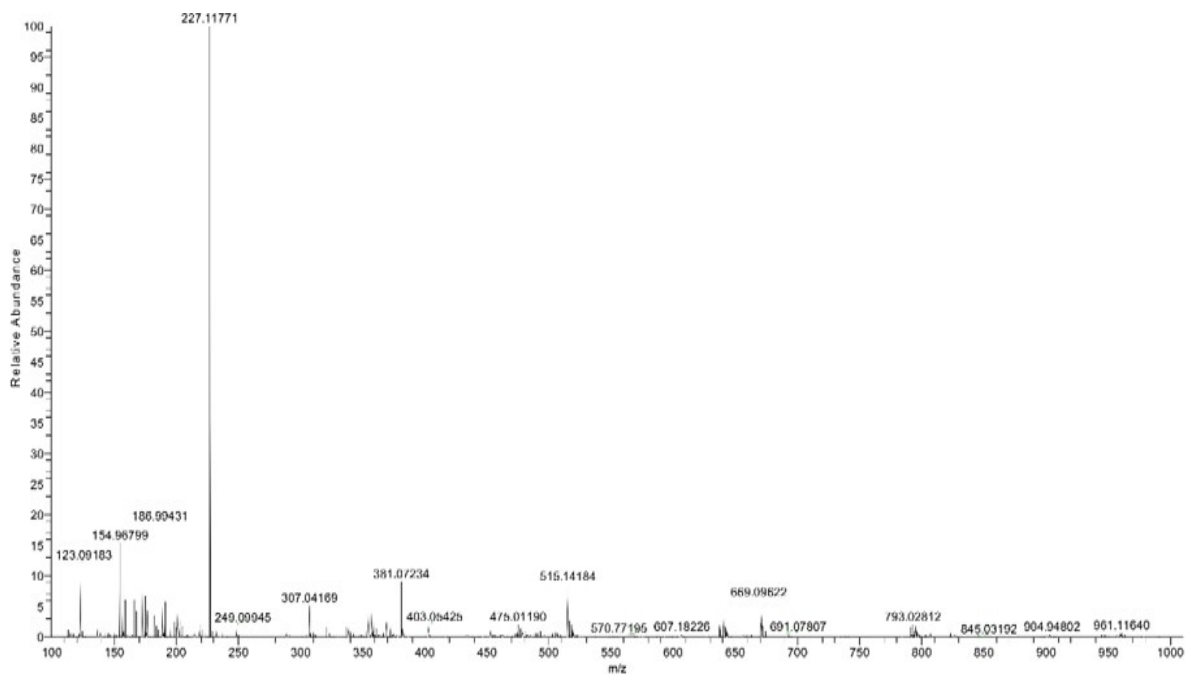


**Figure S12.** HRMS of the complex **ZnL13**.

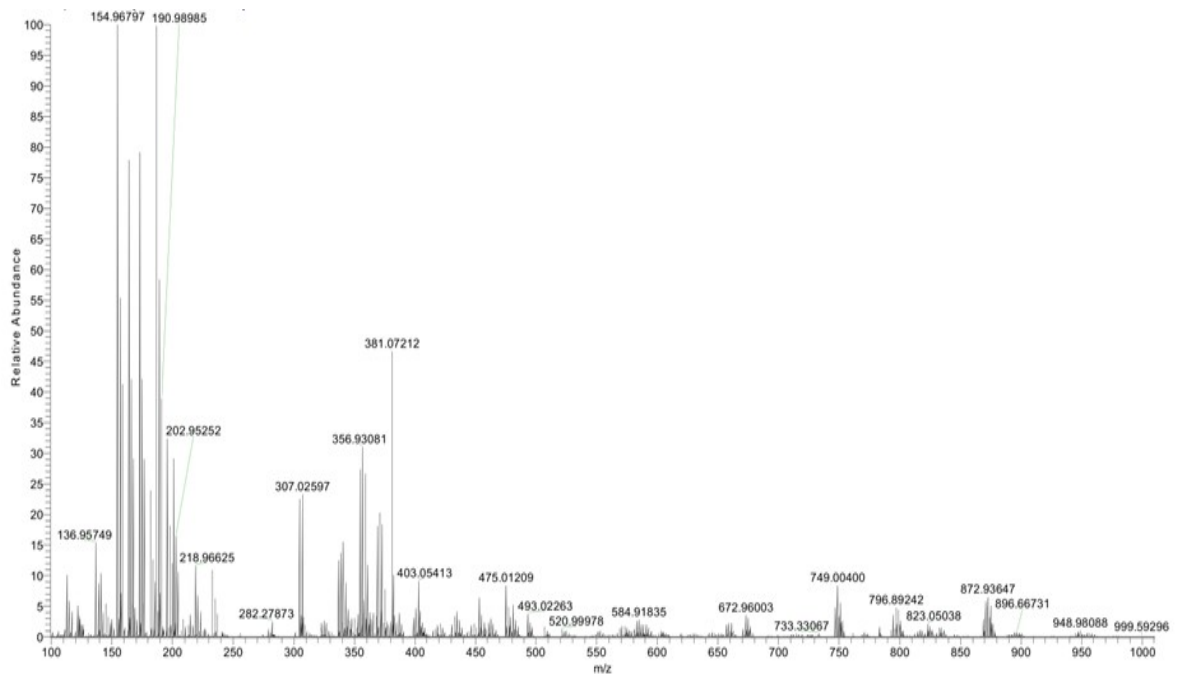


**Figure S13.** HRMS of the complex **ZnL23**.

### TGA analysis

To gather information regarding the Zinc complexes chemical stability for their possible application in optoelectronics, their thermogravimetric curves are presented in Figure S14. It can also be seen in the thermograms that all complexes presented at least two main decomposition processes. The first thermal event showed a temperature of decomposition between 300 to 400 °C, depending on the complex, where the heteroligand presented the higher ones (**ZnL11**: 306 °C, **ZnL22**: 336 °C, **ZnL13**: 342 °C, and **ZnL23**: 342 °C). In this event, the complexes presented initial decomposition temperatures around 300 °C, once again with the heteroligand presenting the higher ones (**ZnL11**: 287 °C, **ZnL22**: 309 °C, **ZnL13**: 313 °C, and **ZnL23**: 317 °C). Firstly, no water or coordinated solvent, usually related to a weight loss between 100-200 °C was observed in the thermograms of the complexes.<sup>1</sup> In addition, around 30% and 15% weight loss could be observed in homo and heteroligands Zn complexes. The second main thermal event takes place between 500-600 °C to a final weight loss between 80-90%. The decomposition of the complexes was not completed at 700 °C, where the final solid material at this temperature is probably a mixture of carbonaceous zinc oxide.

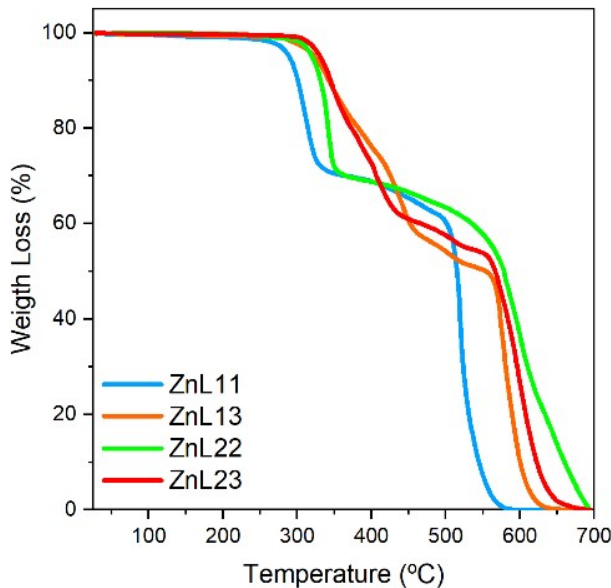


**Figure S14.** TGA thermograms of all complexes.

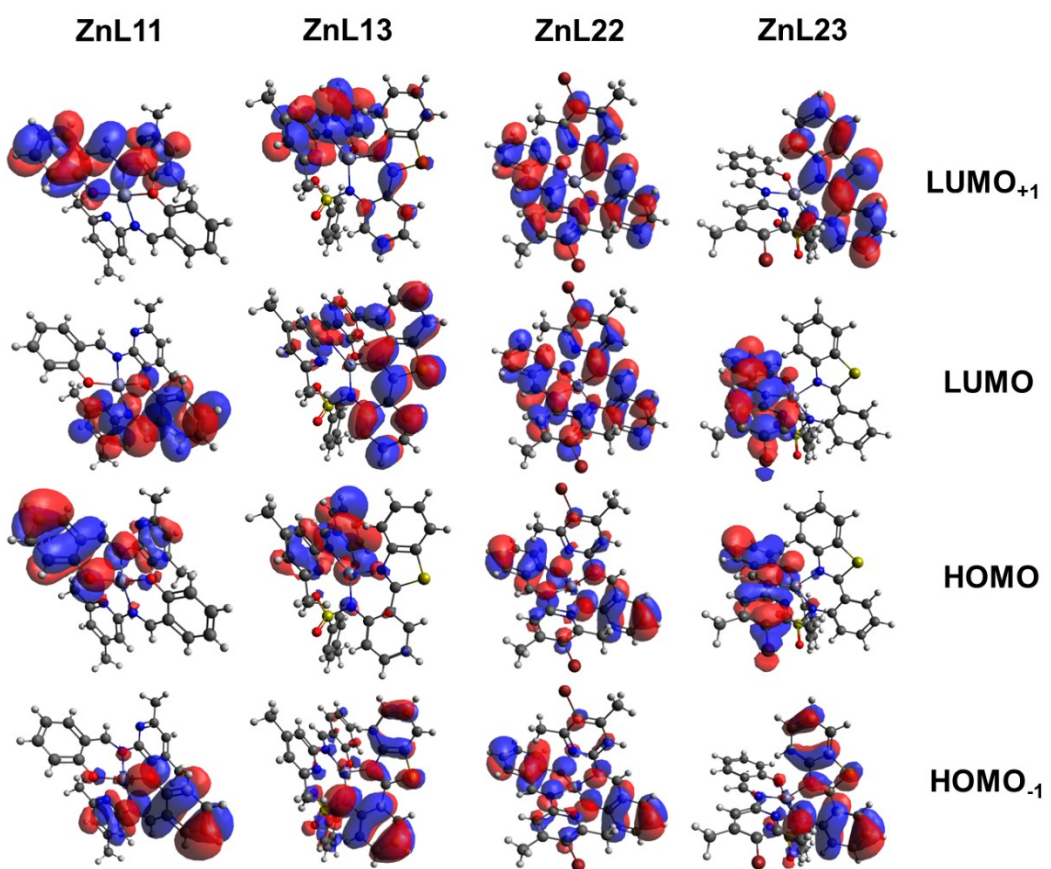


**Figure S15.** Zn(II)-homo and heteroligands HOMO and LUMO frontier molecular orbitals.

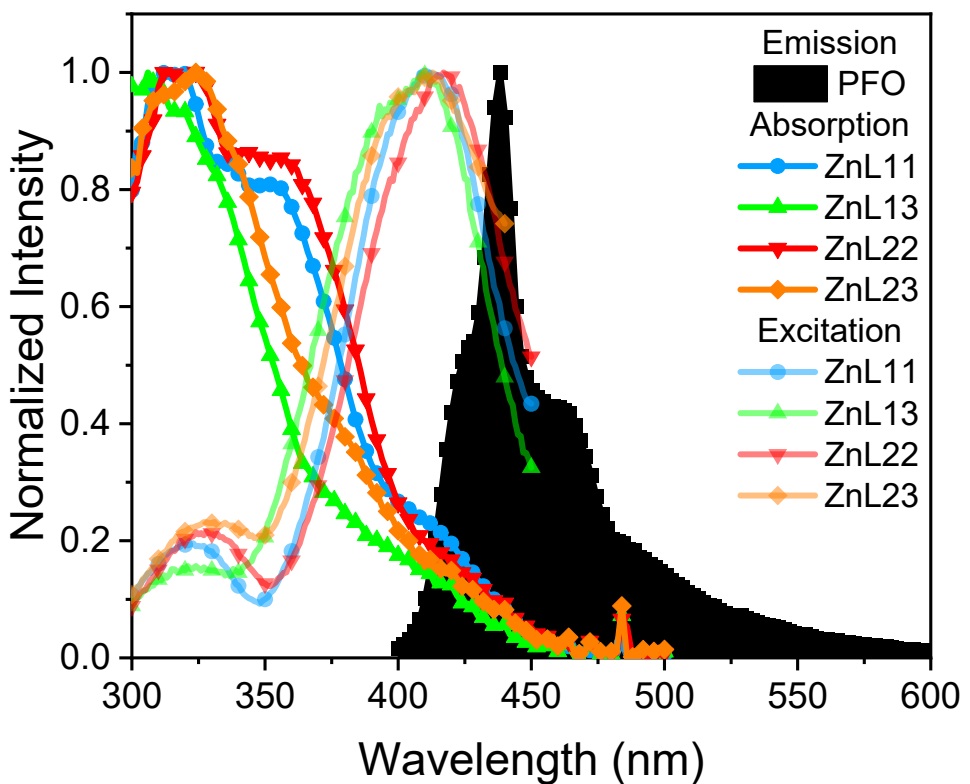


**Figure S16.** Spectral overlap between Zn(II) coordination compounds absorption/excitation and PFO photoluminescence spectra at solid-state and thin-film, respectively.

**Table S2. Summary of time-resolved photoluminescence data used for FRET's efficiencies calculations.**

Film	Conc. (%)	$\tau_1$ (ns)	FRET (%)
<b>PFO</b>		0.278	
<b>ZnL11</b>	0.1	0.250	10
	0.5	0.184	34
	1.0	0.127	54
	2.5	0.089	68
<b>ZnL13</b>	0.1	0.231	17
	0.5	0.166	40
	1.0	0.143	49
	2.5	0.117	58
<b>ZnL22</b>	0.1	0.247	11

	0.5	0.167	40
	1.0	0132	53
	2.5	0.088	68
ZnL23	0.1	0.180	35
	0.5	0.135	51
	1.0	0.123	56
	2.5	0.115	59

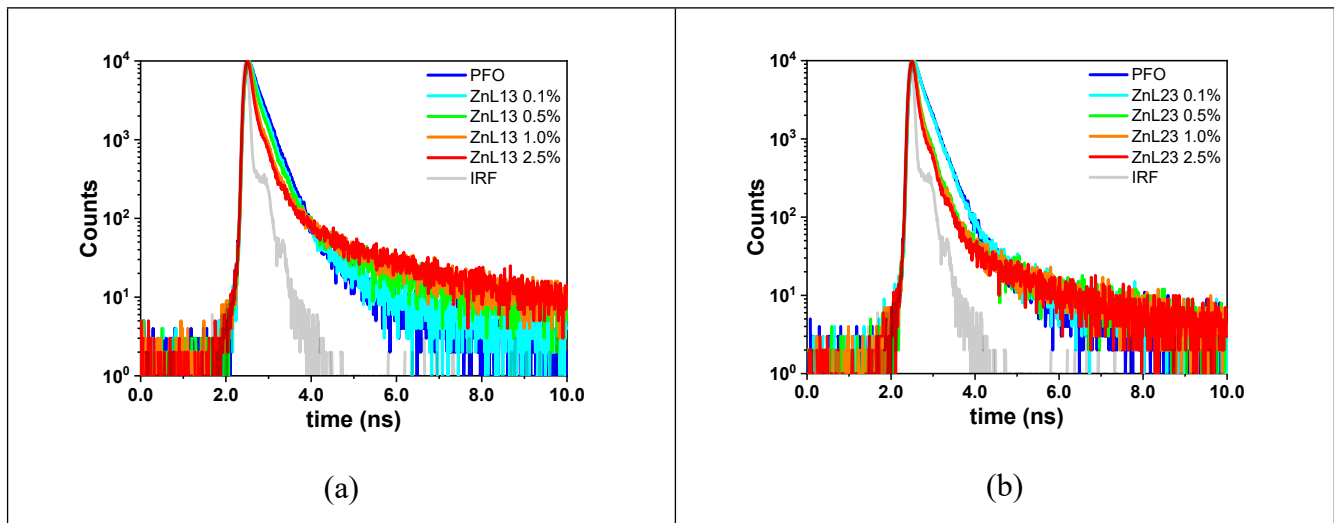


**Figure S17.** Photoluminescence decay curves of (a) **ZnL13** and (b) **ZnL23** at different concentrations in PFO matrix.

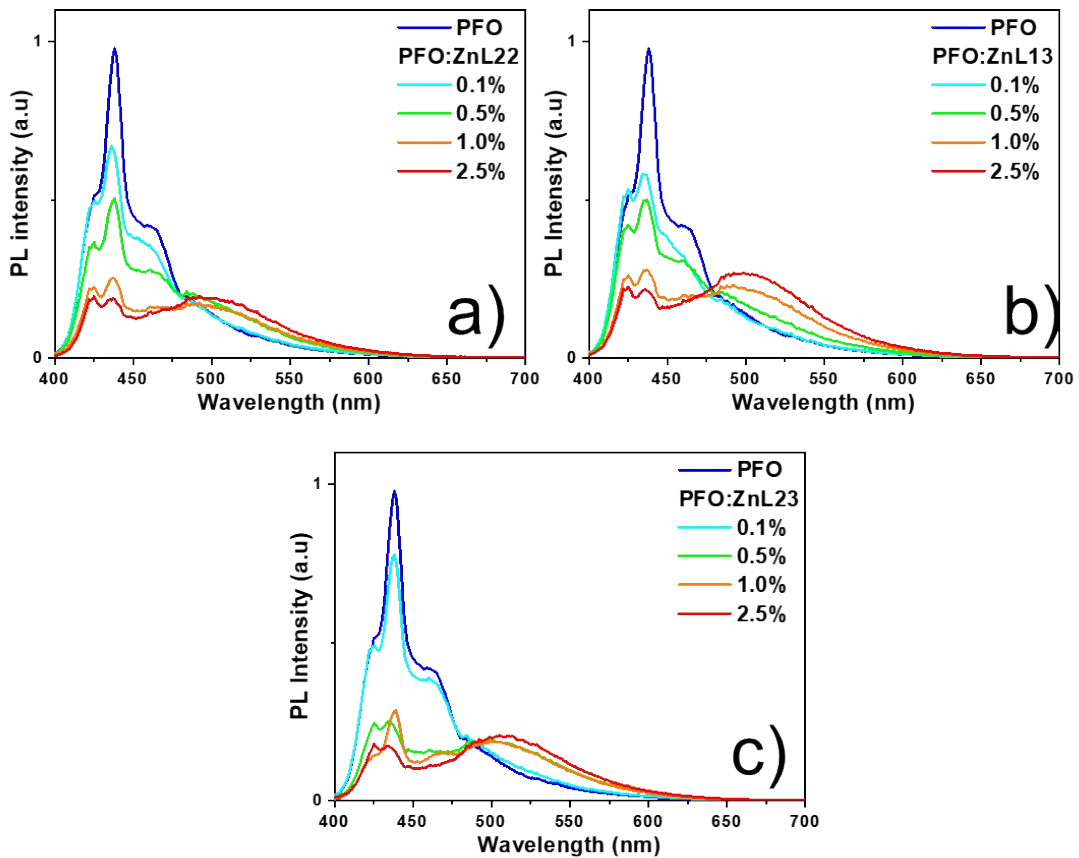


**Figure S18.** Thin film photoluminescence spectra of the Zn(II) coordination compounds excited into PFO matrix ( $\lambda_{\text{exc}}=375$  nm), where: (a) **ZnL22**; (b) **ZnL23**; and (c) **ZnL13**.

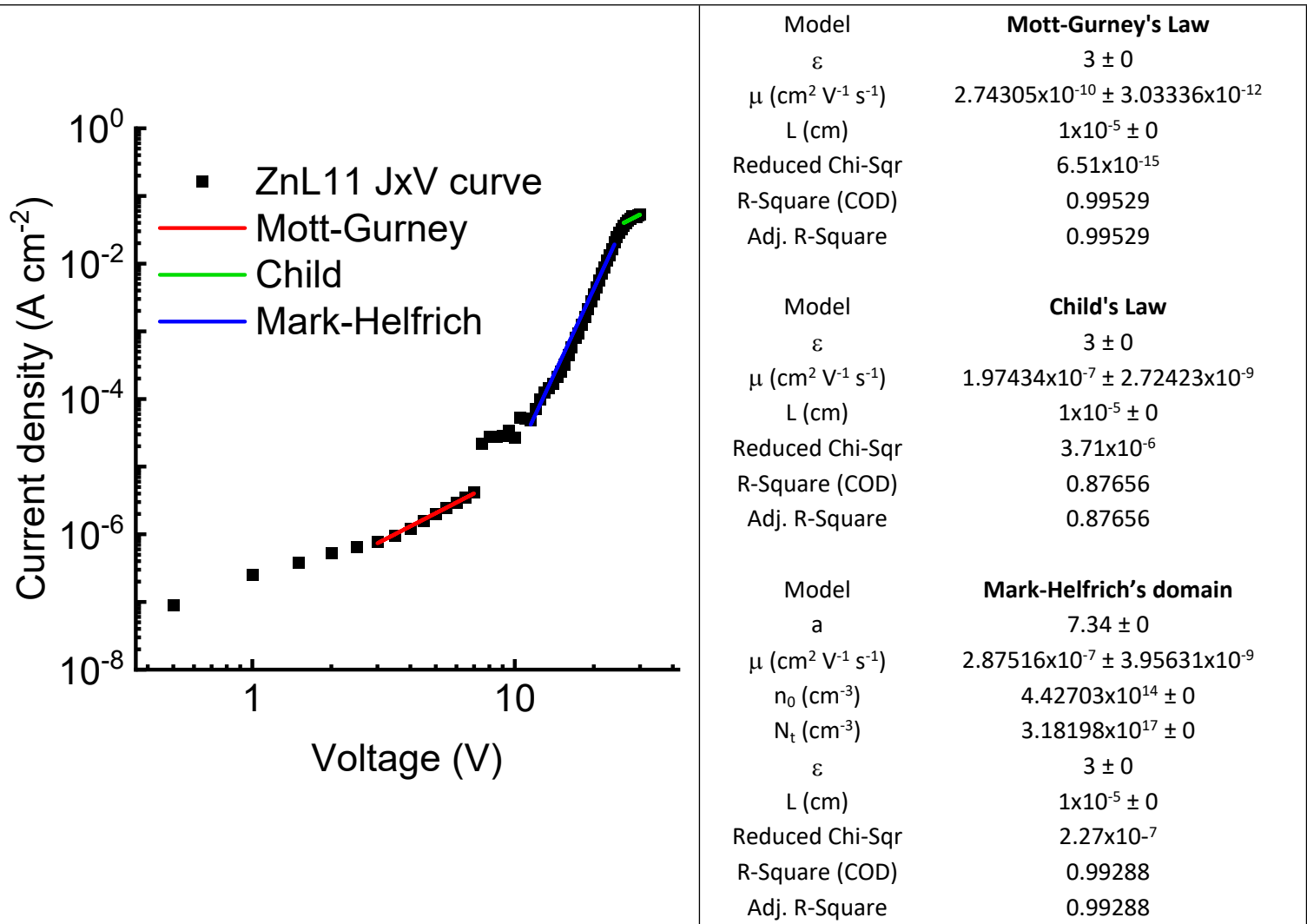
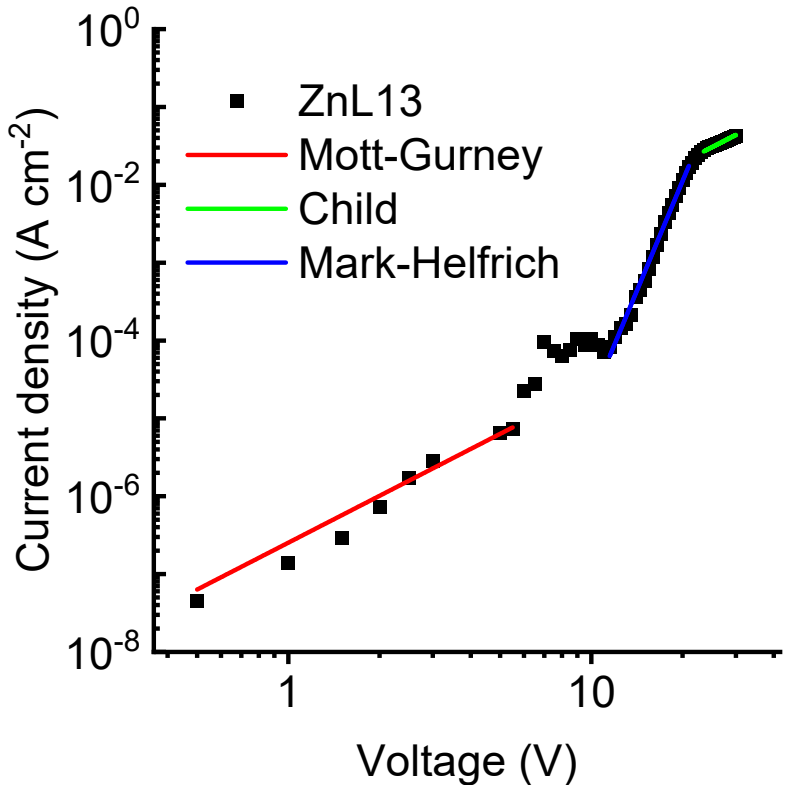


**Figure S19.** Mott-Gurney's, Child's and Mark-Helfrich's space-charge electrical transport models adjusts applied to PFO:ZnL11 (1 % mol/mol) OLED current density versus voltage curve and their fit parameters.



<b>Mott-Gurney's Law</b>	
$\varepsilon$	$3 \pm 0$
$\mu (\text{cm}^2 \text{V}^{-1} \text{s}^{-1})$	$8.4613 \times 10^{-10} \pm 2.26233 \times 10^{-11}$
$L (\text{cm})$	$1 \times 10^{-5} \pm 0$
Reduced Chi-Sqr	$7.68861 \times 10^{-14}$
R-Square (COD)	0.99104
Adj. R-Square	0.99104
<b>Child's Law</b>	
$\varepsilon$	$3 \pm 0$
$\mu (\text{cm}^2 \text{V}^{-1} \text{s}^{-1})$	$1.62541 \times 10^{-7} \pm 1.52177 \times 10^{-9}$
$L (\text{cm})$	$1 \times 10^{-5} \pm 0$
Reduced Chi-Sqr	$1.53299 \times 10^{-6}$
R-Square (COD)	0.91471
Adj. R-Square	0.91471
<b>Mark-Helfrich's domain</b>	
$a$	$8.35 \pm 0$
$\mu (\text{cm}^2 \text{V}^{-1} \text{s}^{-1})$	$2.56541 \times 10^{-7} \pm 2.28384 \times 10^{-9}$
$n_0 (\text{cm}^{-3})$	$1.90124 \times 10^{15} \pm 0$
$N_t (\text{cm}^{-3})$	$3.63326 \times 10^{17} \pm 0$
$\varepsilon$	$3 \pm 0$
$L (\text{cm})$	$1 \times 10^{-5} \pm 0$
Reduced Chi-Sqr	$6.51837 \times 10^{-8}$
R-Square (COD)	0.99753
Adj. R-Square	0.99753

**Figure S20.** Mott-Gurney's, Child's and Mark-Helfrich's space-charge electrical transport models adjust applied to PFO:ZnL13 (1 % mol/mol) OLED current density versus voltage curve and their fit parameters.

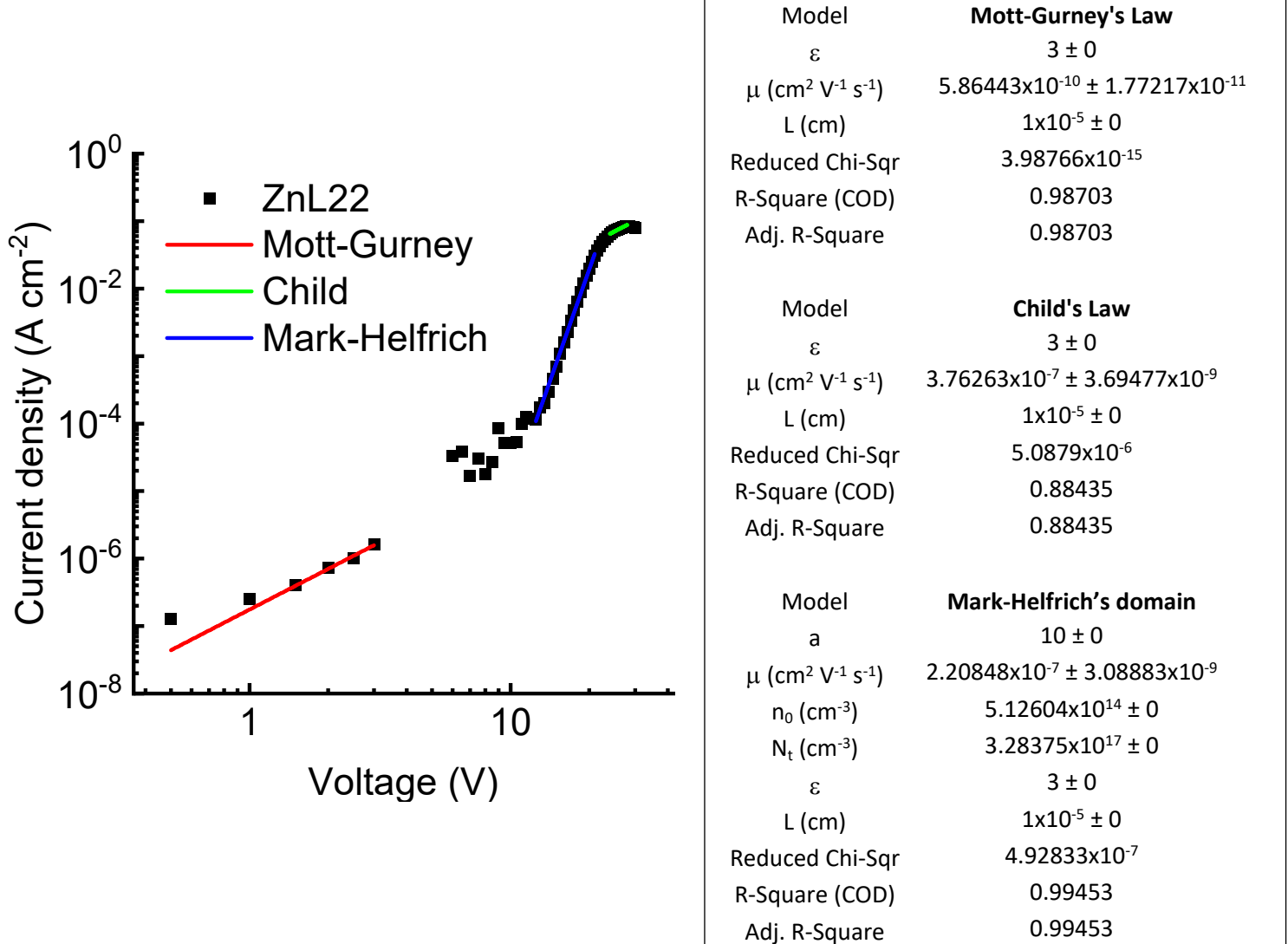


**Figure S21.** Mott-Gurney's, Child's and Mark-Helfrich's space-charge electrical transport models adjusts applied to PFO:ZnL22 (1 % mol/mol) OLED current density versus voltage curve and their fit parameters.

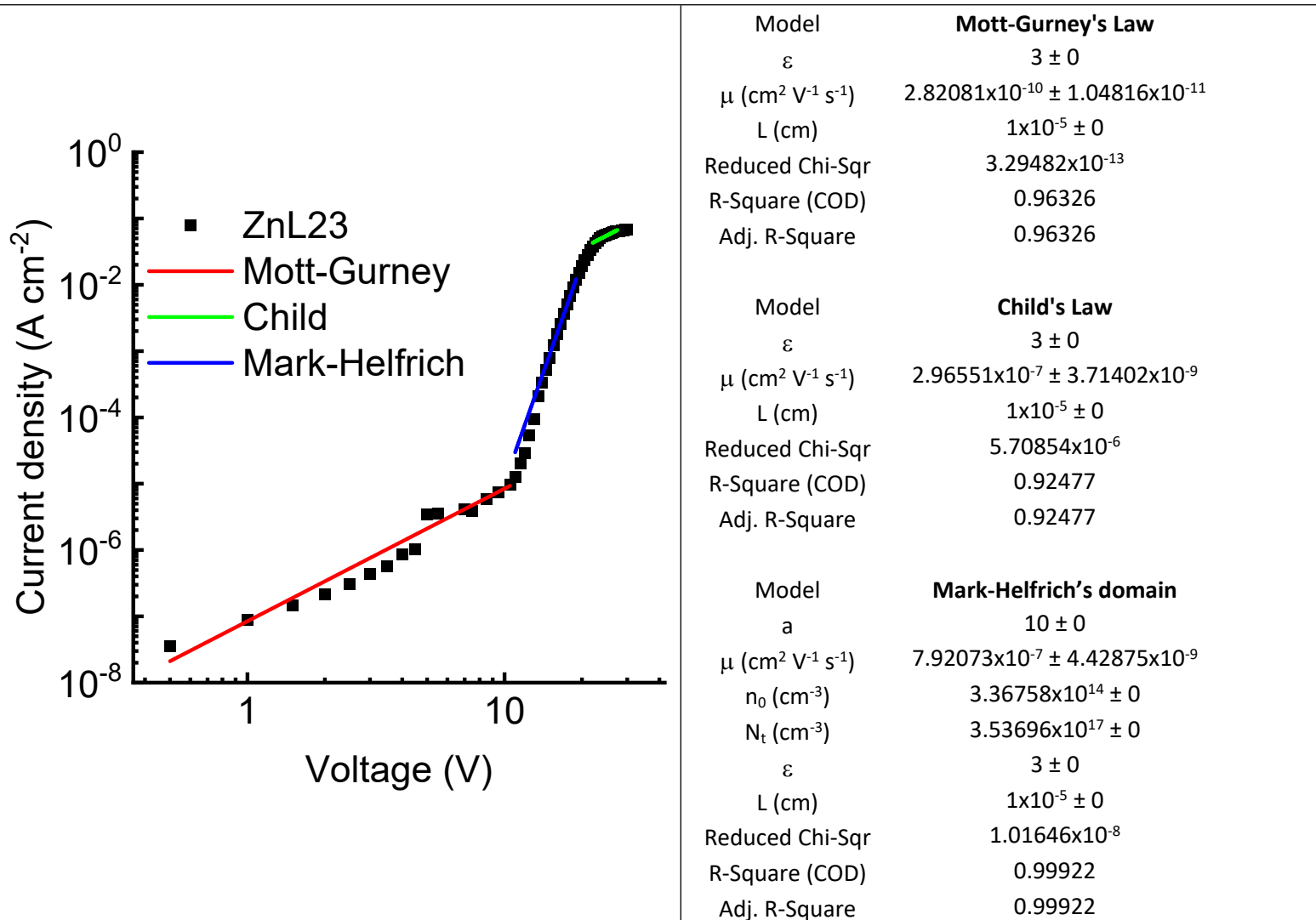


**Figure S22.** Mott-Gurney's, Child's and Mark-Helfrich's space-charge electrical transport models adjust applied to PFO:ZnL2 (1 % mol/mol) OLED current density versus voltage curve and their fit parameters.

## References

- 1 A. Zianna, S. Vecchio, M. Gdaniec, A. Czapik, A. Hatzidimitriou and M. Lalia-Kantouri, in *Journal of Thermal Analysis and Calorimetry*, 2013, vol. 112, pp. 455–464.